Ukrainian Journal of Physical Optics
ISSUE 4
2026

ANNEALING-INDUCED CRYSTALLIZATION OF SILVER THIOARSENITES AND SILVER MIGRATION IN $Ag_x(As_2S_3)_{1-x}$ GLASSES

YU. AZHNIUK [1], A. POGODIN [2], M. FILEP [1,3], V. LOPUSHANSKY[1], V. IZAI [4], V. KRYSHENIK [1], I. VOYNAROVYCH [1], AND A.V. GOMONNAI [1]*

[1] Institute of Electron Physics, Nat. Acad. Sci. Ukr., 21 Universytetska Str., 88017, Uzhhorod, Ukraine
[2] Uzhhorod National University, 3 Narodna Sq., 88000, Uzhhorod, Ukraine
[3] Ferenc Rákóczi II Transcarpathian Hungarian University, 6 Kossuth Sq., Berehovo 90200, Ukraine
[4] Center for Nanotechnology and Advanced Materials, Faculty of Mathematics, Physics and Informatics, Comenius University Bratislava, Mlynská Dolina F1, 84248, Bratislava, Slovakia
*Corresponding author: gomonnai@ukr.net

Received: 11.09.2026

Abstract. X-ray diffraction (XRD) and Raman scattering studies showed that the amorphous structure of $Ag_x(As_2S_3)_{1-x}$ samples with $x \leq 0.15$ is preserved upon annealing at 250 °C for up to 4 h. Meanwhile, XRD patterns of the annealed $x = 0.3$ sample show the presence of three kinds of silver thioarsenite nanocrystals formed in the samples upon annealing: $AgAsS_2$ (smithite and trechmannite) as well as Ag_3AsS_3 (proustite). The average nanocrystal size, estimated from the Scherrer equation, is about 20 nm. Raman spectroscopy also shows the formation of thioarsenite nanocrystals in $Ag_x(As_2S_3)_{1-x}$ glasses upon annealing, with dependence on the silver content and annealing duration. Raman spectroscopy and energy-dispersive X-ray spectroscopy show thermally induced migration of silver atoms toward the sample surface upon annealing.

Keywords: amorphous chalcogenides, phase separation, nanocrystals, X-ray diffraction, Raman spectroscopy, photoinduced effects
UDC: 543.424.2
DOI: 10.3116/16091833/Ukr.J.Phys.Opt.2026.04128

1. Introduction

Ag-containing chalcogenide glasses and thin films have attracted researchers' attention for fundamental studies of their structure and properties because of their optical and thermoelectric characteristics, photosensitivity, and ionic conductivity, which make them promising for applications in optics, optoelectronics, sensorics, and solid-state ionics [1–6]. Ag–As–S system possesses a wide glass-forming region, with the glass compositions mostly prepared along Ag_2S–As_2S_3 [4, 7–10] or Ag–As_2S_3 [5, 11–15] pseudo-binary lines. Much less studied are more sulfur-deficient Ag_3AsS_3–As_2S_3 materials [16–19].

The structure and properties of Ag–As–S glasses are known to undergo substantial changes under illumination. A well-known effect of photodoping As_2S_3 glasses and films with silver is illumination-induced diffusion of Ag atoms preliminarily deposited on the surface into the material depth [12, 13, 20]. Increasing the content of silver in amorphous chalcogenides may lead to substantial changes in their electrical properties, namely, noticeable ionic conductivity, which increases by several orders of magnitude upon the Ag concentration reaching the percolation threshold for ionic transport [21]. The ionic

conductivity is related to an increasing mobility of Ag ions in amorphous Ag–As–S and the formation of channels between the Ag-rich domains.

Formation of nanocrystalline phases in amorphous Ag–As–S attracts interest in view of fundamental studies of the structure, composition, and characteristics of the nanocrystals formed, as well as the effect of nanocrystalline inclusions on the properties of the materials under investigation. Ag_2S nanocrystals uniformly dispersed in amorphous As_2S_3 films were synthesized by diluting As_2S_3 and AgCl in an amine solvent, followed by spin coating [22]. Subsequently, the As_2S_3 films with Ag_2S nanocrystals were used to fabricate nonlinear optical waveguides [23].

This paper presents X-ray diffraction (XRD) and Raman scattering studies of the possible appearance of annealing-induced crystalline phases in $Ag_x(As_2S_3)_{1-x}$ glasses.

2. Experimental

$Ag_x(As_2S_3)_{1-x}$ samples with silver content x up to 0.3 were prepared from pre-synthesized As_2S_3 glass and colloidal silver. We carried out the synthesis at 600°C for 4 h in constantly stirred, evacuated quartz ampoules, followed by rapid quenching in air. Preparation details are provided in our recent study [24]. Samples with silver content x = 0.08, 0.15, and 0.3 were annealed at 250°C for 1 h (batch 1) and 4 h (batch 2). Annealing was carried out using a SNOL muffle furnace (TermoLab), with the temperature controlled by a chromel–alumel thermocouple with an accuracy of ±1 K.

XRD structural analysis of the annealed samples was performed based on the measurements carried out for $Ag_x(As_2S_3)_{1-x}$ samples in Bragg-Brentano configuration using an AXRD Benchtop (Proto Manufacturing Ltd) diffractometer with Cu K_α radiation, a Ni filter, and a Dectris MYTHEN2R microstrip hybrid photon counting detector with 0.5 s exposure at each point.

We performed scanning electron microscopy (SEM) and energy-dispersive X-ray spectroscopy (EDX) using a Tescan Vega TS5136MM scanning electron microscope equipped with an Oxford Instruments INCAx-act EDX detector. We used pure nitrogen (99.99%) at 20 Pa in the specimen chamber as a background gas in middle vacuum mode to avoid surface charging during spectral and EDX mapping measurements. The primary electron beam energy of 20 keV was used for elemental analysis and EDX mapping.

Micro-Raman scattering spectra were recorded for both as-annealed samples and samples subjected to mechanical surface treatment (grinding and polishing). An XPloRa Plus spectrometer (Horiba Scientific) was employed, with excitation by a λ_{exc} = 532 nm solid-state laser at a power density P_{exc} = 4 kW/cm^2. We used a cooled CCD camera to detect the Raman signal. The instrumental resolution was better than 2.5 cm^{-1}. Measurements were performed at room temperature.

3. Results and discussion

Synthesized $Ag_x(As_2S_3)_{1-x}$ samples had an amorphous structure, as confirmed by XRD and Raman spectroscopy [24]. XRD patterns of the annealed $Ag_x(As_2S_3)_{1-x}$ samples are shown in Fig. 1a. It can be seen that samples with x = 0.08 and x = 0.15 exhibit only broad smooth maxima typical for amorphous materials, without any sharp reflection peaks that could indicate the presence of crystalline inclusions. However, for x = 0.3 one can observe a single weak narrow reflection peak at 32.35° (for the sample annealed for τ_{ann} = 1 h) or three

reflection peaks at 28.0°, 32.5°, and 46.4° (for τ_{ann} = 4 h), which are signatures of crystallites formed in the $Ag_{0.3}(As_2S_3)_{0.7}$ glass samples upon annealing. Comparison of the observed diffraction pattern with the reference data for the probable crystalline phases of $AgAsS_2$ – smithite [25] and trechmannite [26], as well as Ag_3AsS_3 – proustite [27] is demonstrated in Fig. 1b. One can see that the observed peaks can originate from any of the three crystalline phases under consideration. The most intense observed narrow peak position (32.5°) almost perfectly matches the corresponding feature of proustite, while the slightly broader peaks at 28.0° and 46.4° can readily originate from contributions of corresponding doublets (27.86° and 28.45° as well as 45.83° and 46.96°). In contrast, the measured diffractogram shows no reflections near the prominent proustite features at 34.98° and 35.90° ([113] and [131] planes, respectively [28]). In general, one may assume the existence of a preferential orientation of the crystallites in the sample which would make the reflections from the [113] and [131] planes less probable; however, one can hardly find a physical reason why the crystallites with such a preferential orientation should be formed in an isotropic glass sample upon annealing. Hence, this is most likely evidence for the absence of the proustite phase in the sample. Another possibility is to ascribe the observed peaks to trechmannite, for which the discrepancies between the characteristic features and the observed peaks are also very tiny (28.27° versus 28.0°, 33.07° versus 32.5°, and 46.75° versus 46.4°). Finally, smithite can also serve a good candidate for the role of the crystalline phase formed, for which the

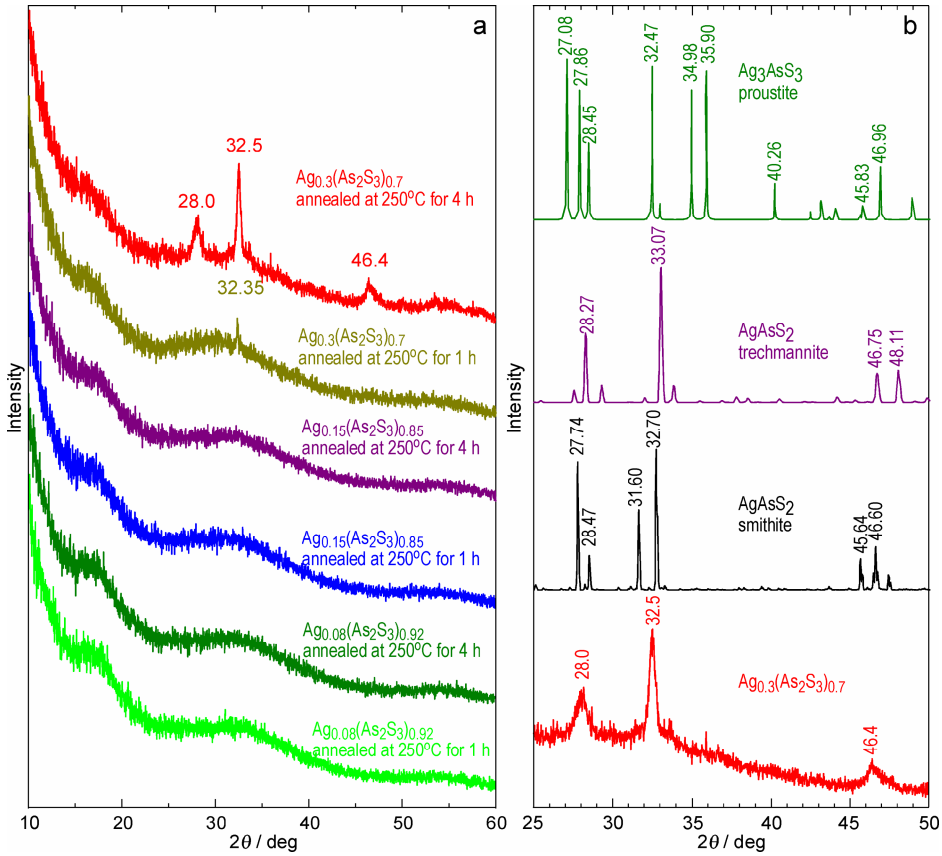

Fig. 1. (a): XRD patterns of annealed $Ag_x(As_2S_3)_{1-x}$ glasses; (b): comparison of the zoomed-in range of the XRD pattern of the annealed $Ag_{0.3}(As_2S_3)_{0.7}$ sample containing the observed reflections to the reference data for possible crystalline phases adapted from the literature (see the text for the references).

intense feature at 32.70° matches the most prominent peak observed at 32.5° while the somewhat broader maxima at 28.0° and 46.4° correspond to the feature at 27.74° (with possible contribution from the one at 28.27°) and a doublet near 45.64° plus a triplet at 46.60°, respectively. The noticeable peak width and low intensity, most likely due to the small crystallite size and the small fraction of atoms participating in crystallization, prevent unambiguous identification of the crystalline phase formed upon annealing.

One should also mention that our recent XRD measurements of unannealed $Ag_x(As_2S_3)_{1-x}$ samples clearly confirmed their amorphous structure for $x \leq 0.3$ while the sample with higher Ag content ($x = 0.4$) rather surprisingly appeared to contain small (up to 50 nm) crystalline inclusions of a relatively rare phase of As_4S_4 – alacranite [24] which, along with the absence of features of elemental silver confirmed the essential role of Ag atoms in building up the Ag–As–S glass network, most likely playing the role of linkages connecting AsS_3 pyramidal units in the glass structure by S–Ag–S bridges [8, 9, 14, 15, 20].

Although, as noted above, we could not unambiguously identify the structure of the crystalline phase formed in the $Ag_{0.3}(As_2S_3)_{0.7}$ samples upon annealing for $\tau_{ann} = 4$ h, we managed to estimate the average size L of the crystallites in the amorphous Ag–As–S matrix based on the halfwidth (FWHM) of the most prominent XRD peak at 32.5°, using the well-known Scherrer equation [29] $\beta(2\theta) = K\lambda / L\cos\theta$ where $\beta(2\theta)$ is the peak halfwidth (for 2θ=32.5° β=0.45°), λ = 0.154 nm is the X-ray wavelength, K is the shape factor (K=0.9), and θ is the diffraction angle. The estimated average crystallite size is about 20 nm.

Illumination can noticeably change the properties of As_2S_3 and Ag–As–S glasses, both due to the thermal effects of absorbed light and to nonthermal photoinduced effects, which are well known for these materials [30–32]. Raman spectra of $Ag_x(As_2S_3)_{1-x}$ glasses may depend on the excitation energy and intensity [24]. In order to minimize photoinduced migration of silver from the illuminated area, which has been reported for amorphous Ag–As–S [7, 12, 13, 20, 24, 33–35], the spectra were measured at a low laser power density P_{exc}= 4 kW/cm², which did not lead to noticeable surface deformation.

Raman spectra of the annealed $Ag_x(As_2S_3)_{1-x}$ glass samples not subjected to post-annealing treatment are shown in Fig. 2. For the glass with $x = 0.08$ one can, similarly to amorphous As_2S_3, observe an intense broad maximum near 340 cm^{-1}, attributed primarily to As–S bond vibrations of AsS_3 (often referred to as $AsS_{3/2}$) pyramidal groups with minor contributions from vibrations of other structural groups [36, 37] as well as two weaker maxima near 180 and slightly below 230 cm^{-1} which are typically assigned to the vibrations of homopolar As–As bonds in As_4S_4 structural groups [37–39]. For the sample with higher Ag content ($x = 0.15$), the dominating feature is observed at a noticeably higher frequency, 356 cm^{-1} (Fig. 2). This maximum is revealed in the Raman spectra of amorphous Ag–As–S materials as the most prominent feature that distinguishes them from amorphous As_2S_3. It is ascribed to the vibrations of As–S bonds in AsS_3 pyramidal units linked by S–Ag–S bridges [8, 9, 14, 15, 20, 40]. For unannealed $Ag_{0.15}(As_2S_3)_{0.85}$ glass, the Raman spectra did not show this feature as a distinct maximum and looked similar to the spectra of glasses with lower Ag content [24]. In any case, Raman spectra of annealed samples with $x < 0.3$ do not show features related to possible crystalline phases that could emerge upon annealing.

From our recent SEM and EDX study [24], it is known that $Ag_x(As_2S_3)_{1-x}$ glasses with $x \geq 0.3$ are composed of quite distinctly separated silver-rich and silver-poor amorphous phases with

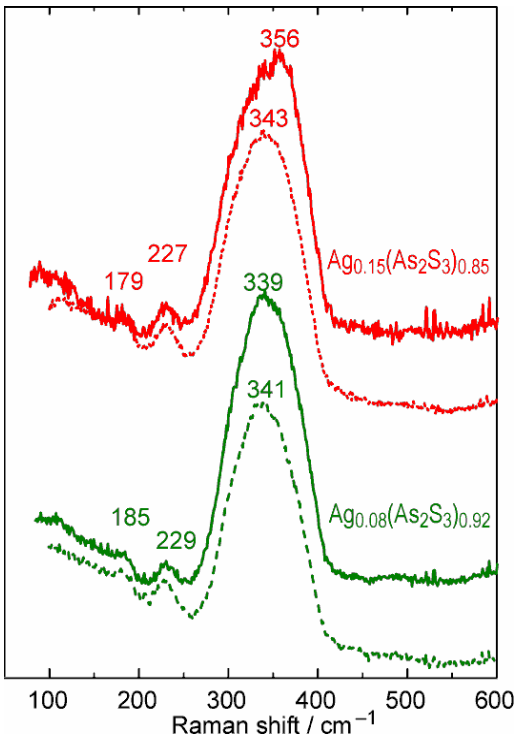

Fig. 2. Solid lines show Raman spectra of $Ag_x(As_2S_3)_{1-x}$ glasses with x = 0.08 and x = 0.15, annealed at 250°C for 1 h and not subjected to any post-annealing treatment, measured at an excitation wavelength of λ_{exc} = 532 nm and P_{exc}=4 kW/cm². Raman spectra of the samples before annealing measured at similar conditions [24] are shown by dotted lines.

a noticeable difference in Ag content (for instance, for x=0.3, nearly 13% versus about 4%, respectively). Earlier studies observed this phase separation at even lower silver content ($x \geq 0.04$) [8, 9]. Silver content in the Ag-rich amorphous phase tends to approach 25 at. % [8], which corresponds to the composition of $AgAsS_2$, the same as that of the known smithite and trechmannite crystals [41].

The EDX mapping of the annealed $Ag_x(As_2S_3)_{1-x}$ glass samples without post-annealing mechanical treatment (Fig. 3) demonstrates that Ag-rich and Ag-poor regions are clearly observed not only for the sample with x = 0.3 (as expected), but also for a much lower silver content (x = 0.15). For the unannealed sample of this composition the element content map was clearly homogeneous [24], The backscattered electron (BSE) images in Fig. 3 confirm the presence and geometrical configuration of areas with different chemical compositions. Backscattered electrons are more intensely reflected by elements with a higher atomic number Z; hence, areas with a higher content of silver (Z=47) appear brighter in the BSE image than those containing more arsenic (Z=33) and sulfur (Z=16).

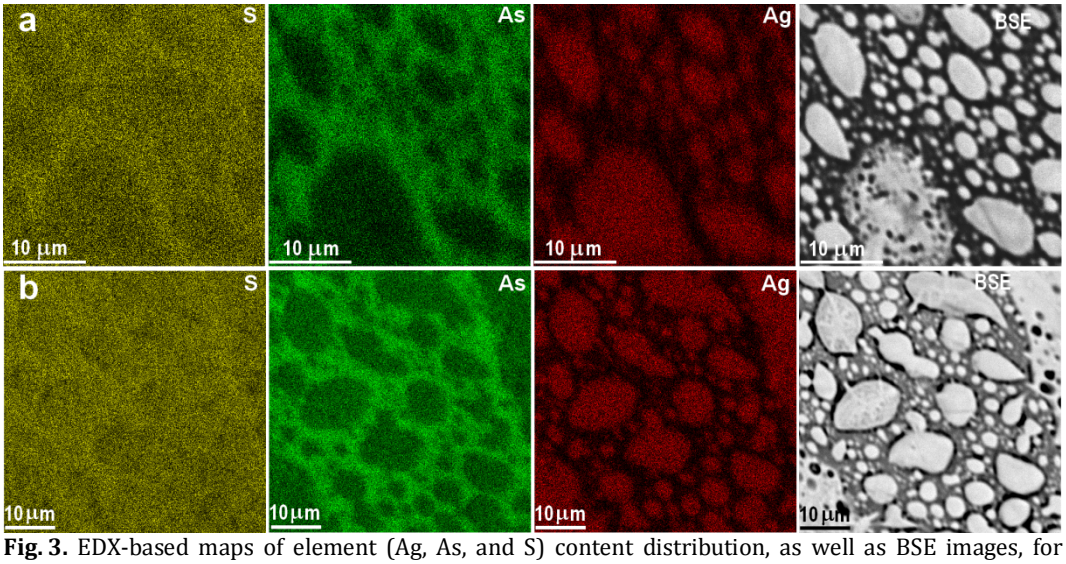

Fig. 3. EDX-based maps of element (Ag, As, and S) content distribution, as well as BSE images, for $Ag_{0.15}(As_2S_3)_{0.85}$ (a) and $Ag_{0.3}(As_2S_3)_{0.7}$ (b) glasses annealed at 250°C for 4 h and not subjected to any post-annealing treatment. Brighter areas indicate a higher content of the relevant element; in the BSE image, brighter areas indicate a higher content of the element with a higher atomic number (Z).

Table 1. EDX-based elemental content in different regions of $Ag_x(As_2S_3)_{1-x}$ glass samples with $x = 0.15$ and $x = 0.3$ annealed at 250 °C for 4 h and not subjected to any post-annealing treatment.

Sample	Ag, at. %	As, at. %	S, at. %
$Ag_{0.15}(As_2S_3)_{0.85}$ (Ag-rich)	23.4	29.1	47.5
$Ag_{0.15}(As_2S_3)_{0.85}$ (Ag-poor)	4.3	38.5	57.2
$Ag_{0.3}(As_2S_3)_{0.7}$ (Ag-rich)	23.6	27.4	49.0
$Ag_{0.3}(As_2S_3)_{0.7}$ (Ag-poor)	4.7	38.5	56.8

The content of the elements of interest in the Ag-rich and Ag-poor regions determined by EDX scanning performed separately over the "bright" and "dark" areas of the annealed samples (Table 1) clearly shows that the Ag-rich and Ag-poor regions within one sample have quite different compositions, but the composition of the Ag-rich (and likewise the Ag-poor) regions is similar for both samples. Similar to the data of our recent study for unannealed samples with $x \geq 0.3$ [24] as well as to those obtained earlier by other authors [8], the silver content in the Ag-rich areas of the annealed samples approaches 25 %, which corresponds to the composition of crystalline smithite and trechmannite $AgAsS_2$. One should point out that both phases, in spite of quite distinct boundaries between them, remain amorphous. Since this separation of the annealed $Ag_x(As_2S_3)_{1-x}$ glasses is revealed for a much broader interval of the sample compositions, one may conclude from the EDX data that the thermal annealing facilitates the separation of the two amorphous phases in $Ag_x(As_2S_3)_{1-x}$.

Other authors [8] observed a coexistence of Ag-rich and Ag-poor amorphous phases in samples across a much wider compositional range (for nominal Ag content above 4 %), whereas our samples before annealing showed phase separation only for $x \geq 0.3$ [24]. This discrepancy may stem from differences in the Ag-to-S content ratio between more sulfur-rich $Ag_x(As_{33}S_{67})_{1-x}$ glasses [8] and $Ag_x(As_2S_3)_{1-x}$ glasses with much less sulfur in our case.

Raman spectra of the unannealed $Ag_{0.3}(As_2S_3)_{0.7}$ sample clearly revealed differences due to phase compositions with different silver content [24]. As could be expected, the spectra of the lighter (Ag-rich) and darker (Ag-poor) regions of annealed samples are also different (Fig. 4). The spectra of the Ag-poor regions clearly show typically

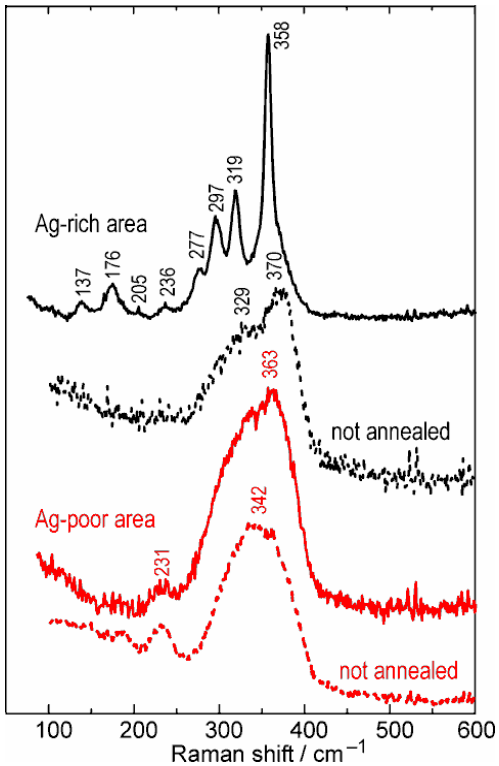

Fig. 4. Solid lines show Raman spectra of Ag-rich and Ag-poor regions of an $Ag_{0.3}(As_2S_3)_{0.7}$ glass sample annealed at 250°C for 1 h and not subjected to any post-annealing treatment. The spectra were measured at an excitation wavelength of $\lambda_{exc} = 532$ nm and $P_{exc} = 4$ kW/cm^2. Raman spectra measured under similar conditions for the Ag-rich and Ag-poor regions of the same sample before annealing [24] are shown by dotted lines.

"amorphous" features with a dominating contribution of the band near 360 cm^{-1}, characteristic of Ag–As–S materials and attributed to the vibrations of As–S bonds in AsS_3 pyramidal units linked by S–Ag–S bridges. Note that this maximum in the Raman spectrum of the Ag-poor areas of the annealed samples is more pronounced than the one for the unannealed sample reported recently [24].

Meanwhile, for the Ag-rich areas of the annealed $Ag_{0.3}(As_2S_3)_{0.7}$ sample (without post-annealing mechanical treatment), the Raman spectra look completely different (Fig. 4). They contain an ample set of narrow Raman peaks evidently corresponding to a crystalline phase (or multiple phases) emerging in the sample upon annealing for 4 h at 250 °C. There are several possible crystalline phases containing Ag, As, and S, the most well-known among them being proustite Ag_3AsS_3, smithite $AgAsS_2$, and trechmannite $AgAsS_2$.

The most intense, highest-frequency narrow peak at 358 cm^{-1} may correspond to proustite (360–364 cm^{-1}) [28, 41, 42], smithite (364 cm^{-1}) [41], and trechmannite (358 cm^{-1}) [41]. However, the unpolarised Raman spectrum of trechmannite is known to contain a very intense dominating narrow peak at 374 cm^{-1} [41] which is missing in our spectrum measured for the Ag-rich region of the annealed $Ag_{0.3}(As_2S_3)_{0.7}$ sample shown in Fig. 4. Since there is no particular reason for any preferred orientation of possibly formed trechmannite crystallites that would prevent the 374 cm^{-1} peak from being revealed in the Raman spectrum, the possibility of formation of trechmannite in the $Ag_{0.3}(As_2S_3)_{0.7}$ glass upon annealing looks less probable, although it cannot be excluded completely since the contribution of the trechmannite feature near 374 cm^{-1} may be masked by other phases contributing to this spectral interval.

Another intense peak at 319 cm^{-1} could correspond to a feature of proustite reported at 318 cm^{-1} [41]; however, for proustite, this peak did not reveal itself as a maximum [28, 41, 42], but was only a component of multi-peak spectrum fitting [41]. Meanwhile, the closest frequency positions of intense peaks are at 332–334 cm^{-1} for proustite [28, 41, 42] and 327 cm^{-1} for smithite [41]. Note that a rather strong and narrow Raman peak at 311–313 cm^{-1} is reported for crystalline As_2S_3 (orpiment) [43–45]. One might assume that orpiment is another crystalline species possibly formed upon annealing of $Ag_{0.3}(As_2S_3)_{0.7}$ glass; however, in such a case the XRD patterns of the annealed samples should contain the most intense orpiment XRD peak at 18.57° [46], which, as can be seen from Fig. 1, is not observed at all. The correct attribution of the Raman peak distinctly observed for the annealed $Ag_{0.3}(As_2S_3)_{0.7}$ sample at 319 cm^{-1} remains unclear.

A clearly defined peak in the spectrum of the annealed $Ag_{0.3}(As_2S_3)_{0.7}$ sample (Ag-rich regions) at 297 cm^{-1} as well as less intense ones at 236 and 277 cm^{-1} do not have clear counterpart in the phonon spectrum of proustite [28, 41, 42] while for smithite an intense peak at 300 cm^{-1} and weaker features at 233 and 280 cm^{-1} are reported [41]. A contribution to the maximum at 236 cm^{-1} may also come from the As–As vibrations in the As_2S_3 glass structure.

The maximum observed at 176 cm^{-1} (Fig. 4) has its counterparts in both proustite (174–185 cm^{-1} [28, 41, 42]) and smithite (177 cm^{-1} [41]) crystals. Likewise, features similar to the weak band at 136 cm^{-1} are reported for proustite (131–132 cm^{-1} [28, 41]) and smithite (142 cm^{-1} [41]).

Based on the Raman measurements, one may suppose that nanocrystals formed upon annealing of $Ag_{0.3}(As_2S_3)_{0.7}$ glass belong to different phases in its Ag-rich regions, namely smithite, proustite, and (less probably) trechmannite. This correlates with the XRD patterns of

the annealed $Ag_{0.3}(As_2S_3)_{0.7}$ sample (Fig. 1), which also show reflections characteristic of the three phases discussed. As mentioned above, XRD data do not unambiguously confirm the presence of proustite crystallites in the annealed sample, although the Raman data suggest a possible contribution. It is generally possible that a small volume fraction of proustite can be insufficient to be detected by XRD, but may simultaneously produce an observable Raman signal. Reliable quantitative estimations of this possibility are strongly encumbered.

An interesting detail was noticed in the Raman spectra of a "mixed' (evidently containing both Ag-rich and Ag-poor areas) region of the $Ag_{0.3}(As_2S_3)_{0.7}$ glass sample annealed at 250°C for 1 h. The spectrum measured at a short acquisition time (20 s) shows a broad feature with a maximum at 364 cm^{-1} and a shoulder near 320 cm^{-1}, as shown in the spectra of the Ag-poor areas of the sample above. However, with increasing acquisition time, narrow features gradually emerge, similar to those revealed in spectra from the Ag-rich areas (Fig. 5). Evidently, these features result from nanocrystal formation in the sample during the measurement. One should note that no such effect was observed for the unannealed sample, nor for annealed samples with lower silver content; with regard to the Ag-rich areas of the same $Ag_{0.3}(As_2S_3)_{0.7}$ glass sample annealed at 250°C for 1 h they were observed immediately, from the very beginning of the measurement (Fig. 4) which means that the formation of nanocrystals was the result of the annealing, but not initiated by the Raman measurement. In this case, the photoinduced formation of the nanocrystals can be related to a purely thermal mechanism driven by the thermal effect of absorption of the incident laser light in the sample and its considerable heating in the laser spot. Similar effects are often observed for bulk and thin-film amorphous chalcogenides [47–54].

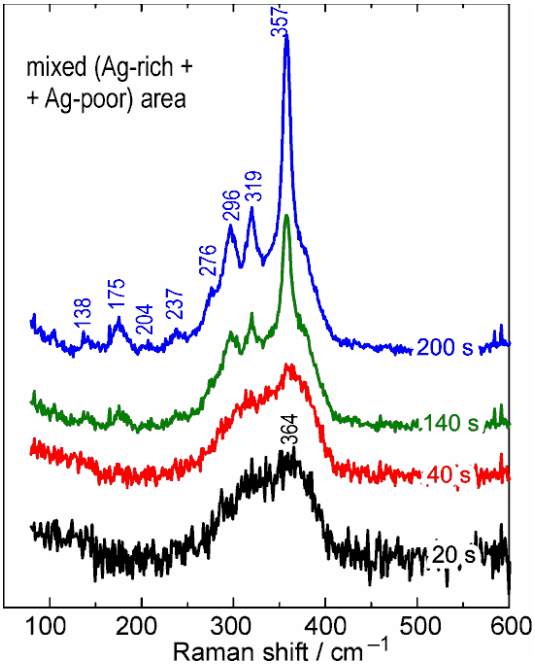

Fig. 5. Time evolution of the Raman spectra of a "mixed' (Ag-rich and Ag-poor) region of an $Ag_{0.3}(As_2S_3)_{0.7}$ glass sample annealed at 250°C for 1 h and not subjected to post-annealing mechanical treatment. We measured the spectra at an excitation wavelength of λ_{exc} = 532 nm and P_{exc} = 4 kW/cm² at different acquisition times.

Alternatively, one may assume a contribution from another mechanism specific to amorphous chalcogenides, where light interaction results in photosoftening of the material and a drastic enhancement of diffusion that can facilitate nanocrystal formation in the illuminated area [55–57]. One should keep in mind that in our case the laser power density (P_{exc}=4 kW/cm²) was much lower than in studies reporting formation of nanocrystals in amorphous chalcogenides due to purely thermal effect of the laser irradiation [50, 51, 54], therefore one may assume that nonthermal photosoftening of the glass structure and photoenhanced diffusion may be to a great extent responsible for the formation of nanocrystals under laser illumination evidenced by Fig. 5.

Raman spectra of the $Ag_{0.3}(As_2S_3)_{0.7}$ glass sample annealed for a longer duration (4 h), shown in Fig. 6, clearly show that narrow features, similar to

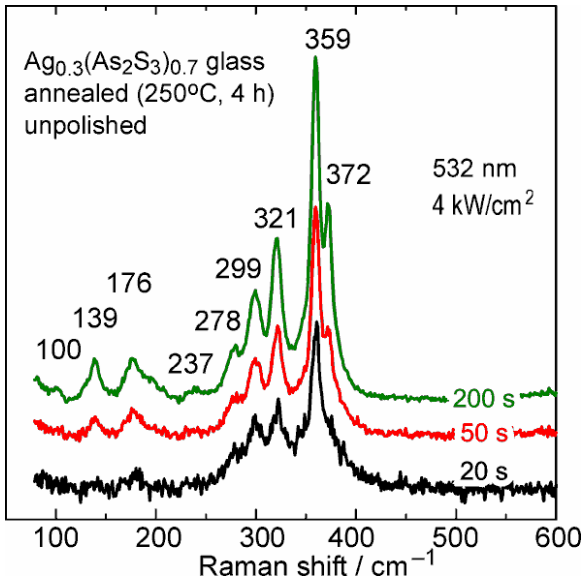

Fig. 6. Time evolution of the Raman spectra of an $Ag_{0.3}(As_2S_3)_{0.7}$ glass sample annealed at 250 °C for 4 h and not subjected to post-annealing mechanical treatment. The spectra were measured at the excitation with λ_{exc}=532 nm, P_{exc}=4 kW/cm².

those observed in the Ag-rich areas of the sample annealed for 1 h, appear from the beginning. They appear in spectra measured at different points on the sample surface, confirming the formation of silver thioarsenite nanocrystals in the annealed samples. The set of narrow Raman features is even more abundant compared to Fig. 4, including the higher-frequency peak at 372 cm^{-1} close to the one characteristic of trechmannite [41], which was not clearly defined for the sample annealed for 1 h. This supports our conclusion that upon annealing of the $Ag_{0.3}(As_2S_3)_{0.7}$ sample, different kinds of silver thioarsenite nanocrystals (smithite, trechmannite, and proustite) are formed. Note that for the $Ag_{0.3}(As_2S_3)_{0.7}$ sample annealed at 250°C for 4 h and not subjected to post-annealing mechanical treatment the spectra measured from different points on the sample surface (presumably Ag-rich and Ag-poor), look practically identical.

All the above spectra were measured for the $Ag_{0.3}(As_2S_3)_{0.7}$ sample, which did not undergo any additional treatment after annealing. When we performed similar measurements after grinding off ~1 mm of the surface layer of the $Ag_{0.3}(As_2S_3)_{0.7}$ sample and polishing, we unexpectedly obtained rather different spectra shown in Fig. 7. For the darker (Ag-poor) regions of the polished sample the dominating Raman maximum was observed at 345 cm^{-1} that correlates with the data for Ag-poor regions of the unannealed sample [24], but does not match the spectrum of the same annealed sample measured before mechanical treatment (Fig. 4) where the spectral position of the peak (363 cm^{-1}) corresponded to a noticeably higher silver content in the Ag-poor region. For the Ag-rich regions of the polished sample, the spectrum also correlates with that of the unannealed sample [24], with the 367 cm^{-1} peak position indicating high Ag content. However, in the spectrum of the annealed sample after the mechanical treatment (grinding and polishing), there is no trace of crystalline features observed for the mechanically untreated annealed sample. From this, one may assume that, in addition to phase separation with coexisting Ag-rich and Ag-poor regions, the inner areas of the sample contain less silver in both Ag-rich and Ag-poor regions. Additionally, comparison of the Raman data in Fig. 4, 6, and 7 implies that thiorsenite nanocrystals are formed upon annealing only in the outer (closer to the surface) parts of the $Ag_{0.3}(As_2S_3)_{0.7}$ sample. Although the annealing was performed in air, there are no indications linking the formation of thioarsenite nanocrystals to oxygen interactions, since both XRD and Raman data clearly show $AgAsS_2$ and crystalline phases but no evidence of oxygen-containing compounds on the sample surface. More extensive experiments are needed to clarify the mechanisms that restrict the formation of thioarsenite nanocrystals in Ag–As–S glasses upon annealing to the near-surface areas of the samples.

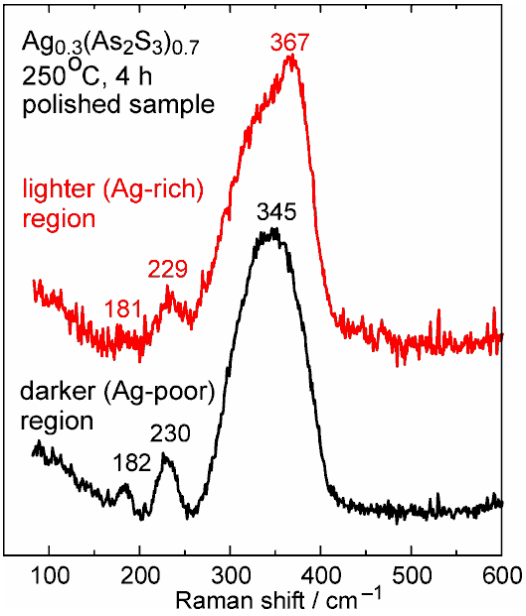

Fig. 7. Raman spectra of Ag-rich and Ag-poor regions of an $Ag_x(As_2S_3)_{1-x}$ glass sample annealed at 250°C for 1 h and polished after the annealing. The spectra were measured at an excitation wavelength of λ_{exc}=532 nm and P_{exc}=4 kW/cm².

EDX mapping measurements of annealed $Ag_x(As_2S_3)_{1-x}$ glass samples subjected to subsequent mechanical treatment (grinding and polishing) also showed noticeably different results from those of annealed samples without surface treatment. As can be seen from Fig. 8a, for the sample with $x = 0.15$, the EDX maps show uniform element content with no visible phase separation into Ag-rich and Ag-poor regions. This pattern is similar to that of the unannealed glass of the same composition [24], but drastically differs from that of the annealed glass with $x = 0.15$ without post-annealing treatment shown in Fig. 3a. Data presented in Table 2 show that the average silver content in the annealed and mechanically treated sample in this case is close to that in the unannealed sample [24] as well as in the Ag-poor regions of annealed $Ag_x(As_2S_3)_{1-x}$ glass samples reported above in Table 1. Meanwhile, for the sample with $x = 0.3$ grinding and polishing do not change the amorphous phase separation pattern (Fig. 8b). Note that, as follows from Table 2, the silver content in the Ag-rich phase of this sample after the post-annealing treatment (13.5 at. %) is close to the one in the silver-enriched region of the unannealed $x = 0.3$ sample (12.7 at. % [24]), but noticeably lower than its value for the Ag-rich area of the annealed sample before the mechanical surface treatment (23.6 at. %, Table 1).

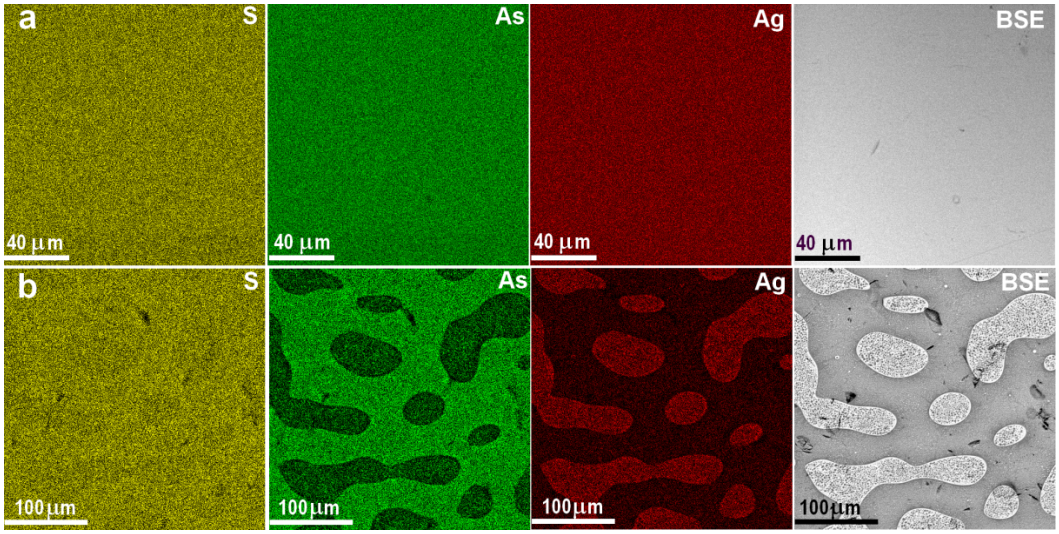

Fig. 8. EDX-based maps of element (Ag, As, and S) content distribution, as well as BSE images for $Ag_{0.15}(As_2S_3)_{0.85}$ (a) and $Ag_{0.3}(As_2S_3)_{0.7}$ (b) glasses annealed at 250 °C for 4 h and subjected to post-annealing surface grinding and polishing. Brighter areas indicate a higher content of the relevant element; in the BSE image, brighter areas indicate a higher content of the element with a higher atomic number (Z).

Table 2. EDX-based elemental content in different regions of $Ag_x(As_2S_3)_{1-x}$ glass samples with x = 0.15 and x = 0.3 annealed at 250 °C for 4 h and polished after the annealing.

Sample	Ag, at. %	As, at. %	S, at. %
$Ag_{0.15}(As_2S_3)_{0.85}$ (no separation)	4.2	38.3	57.5
$Ag_{0.3}(As_2S_3)_{0.7}$ (Ag-rich)	13.5	33.8	52.7
$Ag_{0.3}(As_2S_3)_{0.7}$ (Ag-poor)	5.3	39.0	55.7

It follows from the Raman and EDX data that the initial (untreated) surface and near-surface areas of the annealed samples contain substantially more silver than the inner regions, which are probed by Raman spectroscopy and EDX after the near-surface layer is removed by grinding and polishing. One may conclude that thermal annealing, in particular, results in a noticeable increase in silver migration toward the glass surface.

The contrast between the Ag-rich and Ag-poor phases is well observed not only by SEM [6, 8, 11] and AFM [58] imaging, as well as EDX [24, 59] and micro-Raman [59] mapping, but also by optical microscopy [9]. It can clearly be seen from Fig. 9 that, in our case, annealed $Ag_x(As_2S_3)_{1-x}$ glass samples with $x < 0.3$ are quite homogeneous, while the one with $x = 0.3$, similarly to the unannealed one, clearly demonstrates the presence of geometrically well-defined lighter and darker regions which, similarly to [9], correspond to the regions with higher and lower silver content. These images of the optically resolved Ag-rich and Ag-poor areas on the annealed $Ag_{0.3}(As_2S_3)_{0.7}$ glass surface perfectly match the EDX maps shown in Fig. 8b.

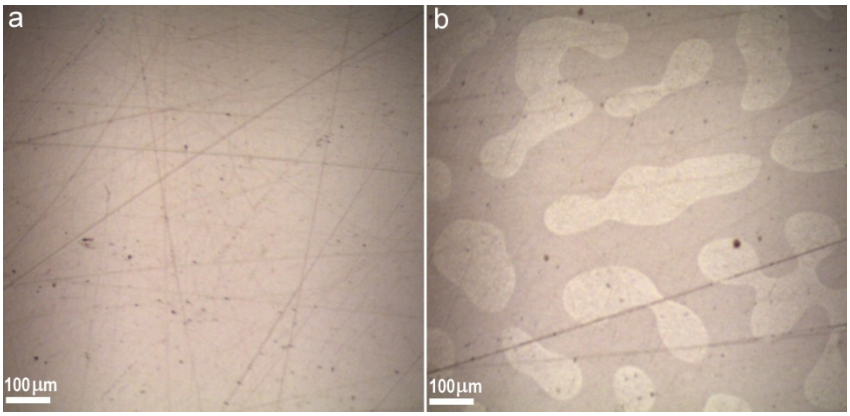

Fig. 9. Optical microscope images of $Ag_{0.15}(As_2S_3)_{0.85}$ (a) and $Ag_{0.3}(As_2S_3)_{0.7}$ (b) glasses annealed at 250 °C for 4 h and polished after the annealing.

4. Conclusions

Amorphous $Ag_x(As_2S_3)_{1-x}$ samples with x up to 0.3 were annealed at 250°C for 1 h and 4 h in a muffle furnace. XRD and Raman scattering studies showed that the amorphous structure of samples with $x \le 0.15$ is preserved upon annealing. Meanwhile, for the annealed $x = 0.3$ sample, the XRD patterns demonstrate the presence of reflections that are characteristic of crystalline silver thioarsenites $AgAsS_2$ (smithite or trechmannite) and Ag_3AsS_3 (proustite). The experimental data are consistent with the formation of all three silver thioarsenite nanocrystal types in the samples upon annealing. The Scherrer equation estimates the average nanocrystal size at about 20 nm.

EDX mapping of the annealed $Ag_x(As_2S_3)_{1-x}$ glasses shows that phase separation into coexisting Ag-rich and Ag-poor amorphous regions is observed not only for samples with

higher silver content (x = 0.3), but also for the sample with x = 0.15, contrary to the unannealed glass of a similar composition.

Raman spectra of the $Ag_{0.3}(As_2S_3)_{0.7}$ sample annealed for 1 h, measured without additional post-annealing mechanical treatment (grinding and polishing) of the sample, demonstrate different behavior for the Ag-rich and Ag-poor areas. Namely, while the Ag-poor areas exhibit broad Raman features typical for amorphous Ag–As–S, the spectra measured from the Ag-rich areas show narrow peaks at frequencies characteristic of smithite, trechmannite, and proustite nanocrystals formed in the amorphous $Ag_{0.3}(As_2S_3)_{0.7}$sample upon annealing. Meanwhile, for the $Ag_{0.3}(As_2S_3)_{0.7}$ sample annealed for 4 h, the nanocrystal-related features are revealed in the spectra measured from different sample points, regardless of the Ag content in the area.

We observed an interesting effect in the $Ag_{0.3}(As_2S_3)_{0.7}$ sample annealed for 1 h. When a "mixed" (Ag-rich + Ag-poor) region of the sample was probed, the Raman spectra initially (at short measurement time) were typical for the amorphous Ag–As–S material, while with increasing measurement time the narrow nanocrystal-related features gradually emerged in the Raman spectra as evidence for the formation of the silver thioarsenite nanocrystals in the laser spot under illumination by the λ_{exc}=532 nm beam. The mechanism of the nanocrystal formation cannot be purely thermal since the laser power density P_{exc}= 4 kW/cm^2 itself is not sufficient for heating the sample to the temperatures required to initiate the material crystallization (otherwise a similar transformation of the spectra could be observed for the unannealed $Ag_{0.3}(As_2S_3)_{0.7}$ sample, which is not the case [24]). Hence, one should consider that an essential role in the photoinduced formation of the silver thioarsenite nanocrystals in the "mixed" area is played by the effect of photosoftening of the Ag–As–S glass, resulting in a drastic drop in its viscosity and enhanced diffusion that enables nanocrystal formation in the illuminated area.

All the above effects were observed for the annealed $Ag_x(As_2S_3)_{1-x}$ samples without any post-annealing mechanical treatment. Raman spectra of the samples after grinding and polishing were typical for amorphous Ag–As–S and did not reveal any signatures of nanocrystal formation. The EDX elemental analysis shows that samples subjected to post-annealing mechanical treatment contain much less silver than the mechanically untreated annealed samples. From this, one may conclude that annealing of $Ag_x(As_2S_3)_{1-x}$ glasses leads to the migration of silver atoms toward the sample surface.

Funding. This work was supported by the "Advanced Science in Ukraine" grant No. 2023.03/0013 from the National Research Foundation of Ukraine.

Conflict of interest. The authors declare no conflicts of interest.

Authors' contribution. Research idea (A. V. Gomonnai). Investigation (Y. Azhniuk, A. Pogodin, M. Filep, V. Lopushansky, V. Izai, I. Voynarovych). Writing – original draft (Y. Azhniuk, V. Kryshenik). Writing – review and editing (Y. Azhniuk, V. Kryshenik, A. V. Gomonnai).

References

1. Frumar, M. & Wagner, T. (2003). Ag doped chalcogenide glasses and their applications. *Curr. Opin. Solid State Mater. Sci. 7*. 117–126.
2. Pradel, A., Kuwata, N., & Ribes, M. (2003). Ion transport and structure in chalcogenide glasses. *J. Phys.: Condens. Matter*. 15. S1561–S1571.
3. Stratan, I., Tsiulyanu, D., & Eisele, I. (2006). A programmable metallization cell based on Ag-As_2S_3. *J. Optoelectron. Adv. Mater. 8*. 2117–2119.

4. Holbrook, C., Chen, P., Novita, D. I., & Boolchand P. (2007). Origin of Conductivity Threshold in the Solid Electrolyte Glass System: $(Ag_2S)_x(As_2S_3)_{1-x}$. *IEEE Transactions on Nanotechnology. 6.* 530–535.
5. Kaban, I., Jóvári, P., Wágner, T., Bartoš, M., Frumar, M., Beuneu, B., Hoyer, W., Mattern, N., & Eckert, J. (2011). Structural study of AsS_2–Ag glasses over a wide concentration range. *J. Non-Cryst. Solids. 357.* 3430–3434.
6. Stehlik, S., Kolar, J., Bartos, M., Vlcek, Mil., Frumar M., Zima, V. & Wagner, T. (2010). Conductivity in Ag–As–S(Se, Te) chalcogenide glasses. *Solid State Ionics. 181.* 1625–1630.
7. Gotoh, T. & Tanaka, K. (2001), Photoinduced surface deformations in ion-conducting Ag–As–S glasses. II. Anisotropic deformation produced by large light spots. *J. Appl. Phys. 89.* 4703–4706.
8. Kyriazis, F., Chrissanthopoulos, A., Dracopoulos, V., Krbal, M., Wagner, T., Frumar, M., & Yannopoulos, S. N. (2009). Effect of silver doping on the structure and phase separation of sulfur-rich As–S glasses: Raman and SEM studies. *J. Non-Cryst. Solids. 355.* 2010–2014.
9. Andrikopoulos, K. S., Arvanitidis, J., Dracopoulos, V., Christofilos, D., Wagner, T., & Yannopoulos, S. N. (2011). Nanoindentation and Raman studies of phase-separated Ag–As–S glasses, *Appl. Phys. Lett. 99*. 171911.
10. Douaud, A., Messaddeq, S. H., & Messaddeq, Y. (2019). Photo-induced birefringence and surface ripples structures in As-S-Ag chalcogenide thin-films. *J. Non-Cryst. Solids. 519.* 119446.
11. Ohta, M., Tsutsumi, M., Izumi, F. & Ueno, S. (1982). Phase separation and structural change accompanying the introduction of silver to arsenic trisulphide glass. *J. Mater. Sci. 17*. 2431–2434.
12. Yaji, T. & Kurita, S. Photodoping sensitivityof Ag into amorphous As_2S_3 films. (1983). *J. Appl. Phys. 54.* 647–651.
13. Indutnyi, I. Z., Dan'ko, V. A., Kudryavtsev, A. A., Michailovskaya, E. V., & Min'ko, V. I. (1995). Photodoping in As_2S_3-Ag structures. *J. Non-Cryst. Solids. 185.* 176–182.
14. Tasseva, J., Todorov, R., Babeva, Tz., & Petkov, K. (2010). Structural and optical characterization of Ag photo-doped thin $As_{40}S_{60-x}Se_x$ films for non-linear applications. *J. Opt. 12.* 065601.
15. Stronski, A., Revutska, L., Meshalkin, A., Paiuk, O., Achimova, E., Korchovyi, A., Shportko, K., Gudymenko, O., Prisacar, A., Gubanova, A., & Triduh, G. (2019). Structural properties of Ag–As–S chalcogenide glasses in phase separation region and their application in holographic grating recording. *Opt. Mater. 94*. 393–397.
16. Okuno, M., Sugaya, H., & Matsumoto, T. (1992). An EXAFS study of Ag_3AsS_3 glass, *J. Non-Cryst. Solids. 150. 356–360.*
17. Studenyak, I. P., Neimet, Yu. Yu., Kranjčec, M., Solomon, A. M., Orliukas, A. F., Kežionis, A., Kazakevičius, E., & Šalkus, T. (2014). Electrical conductivity studies in $(Ag_3AsS_3)_x(As_2S_3)_{1-x}$ superionic glasses and composites. *J. Appl. Phys. 115.* 033702.
18. Studenyak, I., P., Neimet, Yu.,Yu., Rati, Y., Y., Stanko, D., Kranjčec, M., Kökényesi, S., Daróci, L., & Bohdan, R. (2014.) Structural and optical properties of annealed and illuminated $(Ag_3AsS_3)_{0.6}(As_2S_3)_{0.4}$ thin films. *Opt. Mater. 37.* 718–723.
19. Studenyak, I. P., Molnar, Z. R., Kutsyk, M. M., Izai, V. Yu., Kranjčec, M., & Kökényesi, S. (2018). Temperature studies of optical absorption in the sandwich structure based on $(Ag_3AsS_3)_{0.6}(As_2S_3)_{0.4}$ thin film and gold nanoparticles. *Semicond. Phys., Quantum Electron. & Optoelectron. 21.* 89–94.
20. Wágner, T., Vlček, Mir., Kasap, S. O., Vlček, Mil., & Frumar, M. (2001), Changing the composition of Ag–As–S amorphous films using photo-induced solid state reaction. *J. Non-Cryst. Solids. 284.* 168–173.
21. Piarristeguy, A., Ramonda, M., Kuwata, N., Pradel, A., & Ribes, M. (2006). Microstructure of Ag_2S–As_2S_3 glasses. *Solid State Ionics. 177.* 3157–3160.
22. Almeida, J. M. P., Lu, C., Mendonça, C. R., & Arnold, C. B. (2015), Single-step synthesis of silver sulfide nanocrystals in arsenic trisulfide. *Opt. Mater. Expr. 5*. 1815–1821.
23. Almeida, J. M. P., Barbano, E. C., Arnold, C. B., Misoguti, L., & Mendonça, C. R. (2017). Nonlinear optical waveguides in As_2S_3-Ag_2S chalcogenide glass thin films. *Opt. Mater. Expr. 7*. 93–99.
24. Azhniuk, Y., Pogodin, A., Izai, V., Filep, M., Lopushansky, V., Satrapinskyy, L., Yukhymchuk, V., Kryshenik, V., Voynarovych, I., & Gomonnai, A. V. (2025). Phase separation and photoinduced migration of silver in $Ag_x(As_2S_3)_{1-x}$ glasses. *Mater. Res. Expr. 12.* 095201.
25. Hellner, E., & Burzlaff, H. (1964). Die Struktur des Smithits $AgAsS_2$. *Naturwissenschaften. 51.* 35–36.
26. Matsumoto, T., & Nowacki, W. (1969). The crystal structure of trechmannite, $AgAsS_2$. *Zeitschrift für Kristallographie. 129.* 163–177.
27. Allen, S. (1985). Phase transitions in proustite I. Structural studies. *Phase Transitions. 6.* 1–24.

28. Smitiukh, O. V., Marchuk, O. V., Kogut, Y. M., Yukhymchuk, V. O., Mazur, N. V., Myronchuk, G. L., Ponedelnyk, S. M., Cherniushok, O. I., Parashchuk, T. O., Khyzhun, O. Y., Wojciechowski, K. T., & Fedorchuk, A. O. (2022). Effect of rare-earth doping on the structural and optical properties of the Ag_3AsS_3 crystals. *Opt Quant Electron. 54*. 224.
29. Scherrer, P. (1918). Bestimmung der Größe und der inneren Struktur von Kolloidteilchen Mittels Röntgenstrahlen. *Nachr. Ges. Wiss. Göttingen, Math. - Phys. Klasse. 1918*. 98.
30. Tanaka, K. (2014). Photoinduced deformations in chalcogenide glasses, in: R.P. Wang (Ed.), Amorphous Chalcogenides: Advances and Applications, *Pan Stanford Publishing*. 59-96.
31. Tanaka K., & Shimakawa K. (2021). Amorphous Chalcogenide Semiconductors and Related Materials. *Springer Nature Switzerland AG.Cham.*
32. Yannopoulos, S., N. (2021). Athermal photoelectronic effects in non-crystalline chalcogenides: Current status and beyond, in: A.V. Kolobov and K. Shimakawa (Ed.). The World Scientific Reference of Amorphous Materials: Structure, Properties, Modeling and Applications (Volume 1: Chalcogenide Glasses). *World Scientific Publishing. Singapore.* 251–311.
33. Kovalskiy, A., Ganjoo, A., Khalid, S., & Jain, H. (2010). Combined high-resolution XPS and EXAFS study of Ag photodissolution in a-As_2S_3 thin film. *J. Non-Cryst. Solids. 356.* 2332–2336.
34. Lőrinczi, A., Popescu, M., Sava, F., Velea, A., & Şimăndan, I.-D. (2011). Silver doped As_2S_3 chalcogenide films: A diffusion study. *Phys. Status Solidi C. 8.* 2617–2620.
35. Indutnyi, I. Z., Mynko, V. I., Sopinskyy, M. V., & Mamykin, S. V. (2025). Surface plasmon-polariton study of photoinduced diffusion in light-sensitive Ag–As_2S_3 thin-film structure. *Thin Solid Films. 824.* 140705.
36. Chen, P., Holbrook, C., Boolchand, P., Georgiev, D. G., Jackson, K. A., & Micoulaut, M. (2008). Intermediate phase, network demixing, boson and floppy modes, and compositional trends in glass transition temperatures of binary As_xS_{1-x} system. *Phys. Rev. B. 78.* 224208.
37. Yannopoulos, S. N., Andrikopoulos, K. S., Kastrissios, D. Th., & Papatheodorou, G. N. (2012). Origin of photoinduced defects in glassy As_2S_3 under band gap illumination studied by Raman scattering: A revisory approach. *Phys. Status Solidi B. 249.* 2005–2012.
38. Frumar, M., Jedelský, J., Frumarová, B., Wágner, T., & Hrdlička, M. (2003), Optically and thermally induced changes of structure, linear and non-linear optical properties of chalcogenides thin films. *J. Non-Cryst. Solids. 326–327*. 399–404.
39. Yannopoulos, S. N. (2003). Intramolecular structural model for photoinduced plasticity in chalcogenide glasses. *Phys. Rev. B. 68*. 064206.
40. Firth, A., Owen A., & Ewen, P. (1981). Laser-Raman study of the structure of silver doped $As_{40}S_{60}$ glass. *Journal de Physique Colloques 42*. C4-903–C4-906.
41. Kharbish, S. (2017). Spectral-structural characteristics of the extremely scarce silver arsenic sulfosalts, proustite, smithite, trechmannite and xanthoconite: μ-Raman spectroscopy evidence. *Spectrochim. Acta A Mol. Biomol. Spectrosc. 177*. 104–110.
42. Makreski, P., Jovanovski, G., Minceva-Sukarova, B., Soptrajanov, B., Green, A., Engelen, B., & Grzetic, I. (2004). Vibrational spectra of $M^I_3M^{III}S_3$ type synthetic minerals (M^I = Tl or Ag and M^{III} = As or Sb). *Vibrational Spectroscopy. 35.* 59–65.
43. Forneris, R. (1969). The infrared and Raman spectra of realgar and orpiment. *Amer. Mineralog. 54.* 1062–1074.
44. Zallen, R., Slade, M. L., & Ward, A. T. (1971). Lattice vibrations and interlayer interactions in crystalline As_2S_3 and As_2Se_3. *Phys. Rev. B. 3.* 4257–4273.
45. Černošek, Z., Černošková, E., & Beneš, L. (1999) Crystalline arsenic trisulfide: preparation, differential scanning calorimetry and Raman scattering measurements. *Mater. Lett. 38*. 336–340.
46. Liu, K., Dai, L., Li, H., Hu, H., Yang, L., Pu, C., Hong, M., & Liu, P. (2019). Phase transition and metallization of orpiment by Raman spectroscopy, electrical conductivity and theoretical calculation under high pressure. *Materials. 12.* 784–796.
47. Kolev, K., & Wautelet, M. (1990). Kinetics of CW laser-induced crystallization and oxidation of thin Sb, Se, and Sb_2Se_3 films in air. *Appl. Phys. A. 50.* 192–196.
48. Azhniuk, Yu. M., Stoyka, V., Petryshynets, I., Rubish, V. M., Guranich, O. G., Gomonnai, A. V., & Zahn, D. R. T. (2012). SbSI nanocrystal formation in As–Sb–S–I glass under laser beam. *Mater. Res. Bull. 47*. 1520–1522.
49. Makreski, P., Petruševski, G., Ugarković, S., & Jovanovski, G. (2013). Laser-induced transformation of stibnite (Sb_2S_3) and other structurally related salts. *Vibr. Spectrosc. 68*. 177–182.
50. Azhniuk, Yu. M., Gomonnai, A. V., Rubish, V. M., Rigan, M. Yu., Solomon, A. M., Gomonnai, O. O., Guranich, O. G., Petryshynets, I., & Zahn, D. R. T. (2013). *In situ* Raman observation of laser-induced formation of $TlInSe_2$ crystallites in Tl–In–As–Se glass. *J. Phys. Chem. Solids. 74.* 1452–1458.

51. Azhniuk, Y. M., Gomonnai, A. V., Lopushansky, V. V., Gomonnai, O. O., Babuka, T., Loya, V. Y., & Voynarovych, I. M. (2023). Laser-induced transformations in thermally evaporated thin $TlInSe_2$ films studied by Raman spectroscopy. *Ukr. J. Phys. 68*. 816–821.
52. Azhniuk, Y., Hasynets, S., Lopushansky, V., Kryshenik, V., Solomon, A. M., & Gomonnai, A. V. (2023). Raman study of photoinduced crystallization of SnS_2 in As_2S_3:Sn glasses. *Vibr. Spectrosc. 128.* 103583.
53. Azhniuk, Y. M., Lopushansky, V. V., Loya, V. Y., Hasynets, S. M., Kryshenik, V. M., & Gomonnai, A. V. (2026). Formation of SnS_2 nanocrystals in amorphous $(As_2S_3)_{1-x}(SnS_2)_x$ films studied by Raman spectroscopy. *Molecular Cryst. Liquid Cryst. 770.* 907 – 919.
54. Fernandes, Th., Hans, P., Texier, M., Comby-Dassonneville, S., Mariette, C., Mignerot, F., Jeannot, S., le Friec, Y., Simola, R., & Thomas, O. (2025), Laser-induced crystallization and amorphization of Ge-Rich GST thin films monitored in situ with synchrotron X-ray diffraction. *Phys. Stat. Solidi RRL. 19.* 2400392.
55. Azhniuk, Yu. M., Dzhagan, V. M., Solonenko, D., Mukherjee, A., Loya, V. Yu., Grytsyshche, I. V., Lopushansky, V. V., Gomonnai, A. V., & Zahn, D. R. T. (2019). Laser annealing-induced formation of CdS nanocrystals in Cd-doped amorphous As_2S_3 thin films. *Phys. Status Solidi B. 256.* 1800298.
56. Azhniuk, Y. M., Lopushansky, V. V., Loya, V. Yu., Kryshenik, V. M., Dzhagan, V. M., Gomonnai, A. V., & Zahn, D. R. T. (2020). Raman study of laser-induced formation of II–VI nanocrystals in zinc-doped As–S(Se) films. *Appl. Nanosci. 10.* 4831–4837.
57. Azhniuk, Y. M., Dzhagan, V. M., Solonenko, D. Lopushansky, V. V., Loya, V. Y., Kryshenik, V. M., Voynarovych, I. M., Gomonnai, A. V., & Zahn, D. R. T. (2021). Ternary $CdS_{1-x}Se_x$ nanocrystals formed in Cd-doped As–Se–S films due to photoenhanced diffusion during micro-Raman measurement. *J. Raman Spectrosc. 52.* 821–832.
58. Stehlik, S., Kolar, J., Frumar, M., Wagner, T., Haneda, H., & Sakaguchi, I. (2011). Phase separation in chalcogenide glasses: the system AgAsSSe. *Int. J. Appl. Glass Sci. 2.* 301–307.
59. Correr, W., Messaddeq, S. H., Douaud, A., & Messaddeq, Y. (2021). Vibrational and conductive microscopic investigation of thermal dewetting in Ag-As-S chalcogenide thin films. *Appl. Surf. Sci. 554.* 149621.

Azhniuk, Yu., Pogodin, A., Filep, M., Lopushansky, V., Izai, V., Kryshenik, V., Voynarovych, I., and Gomonnai A.V. (2026). Annealing-Induced Crystallization of Silver Thioarsenites and Silver Migration in $Ag_x(As_2S_3)_{1-x}$ Glasses. *Ukrainian Journal of Physical Optics*, *27*(4), 04128 – 04142. doi: 0.3116/16091833/Ukr.J.Phys.Opt.2026.04128

Анотація. *Дослідження дифракції рентгенівських променів і раманівської спектроскопії показали, що при відпалі при 250 °C тривалістю до 4 год зберігається аморфна структура зразків $Ag_x(As_2S_3)_{1-x}$ з $x \geq 0.15$. Водночас дифрактограми зразка з $x = 0.3$ вказують на утворення при відпалі нанокристалів тіоарсенатів срібла трьох типів: $AgAsS_2$ (смітит і трехманіт) та Ag_3AsS_3 (пристит). Середній розмір утворених нанокристалів, оцінений за формулою Шерера, становить близько 20 нм. Утворення нанокристалів тіоарсенітів у склах $Ag_x(As_2S_3)_{1-x}$ при відпалі також підтверджується даними раманівської спектроскопії, яка показує залежність цього явища від вмісту срібла у склі та тривалості відпалу. Методами раманівської спектроскопії та енергодисперсійної рентгенівської спектроскопії показано термоіндуковану міграцію срібла з об'єму до поверхні зразків.*

Ключові слова: *аморфні халькогеніди; розділення фаз; нанокристали; дифракція рентгенівських променів; раманівська спектроскопія; фотоіндуковані ефекти*